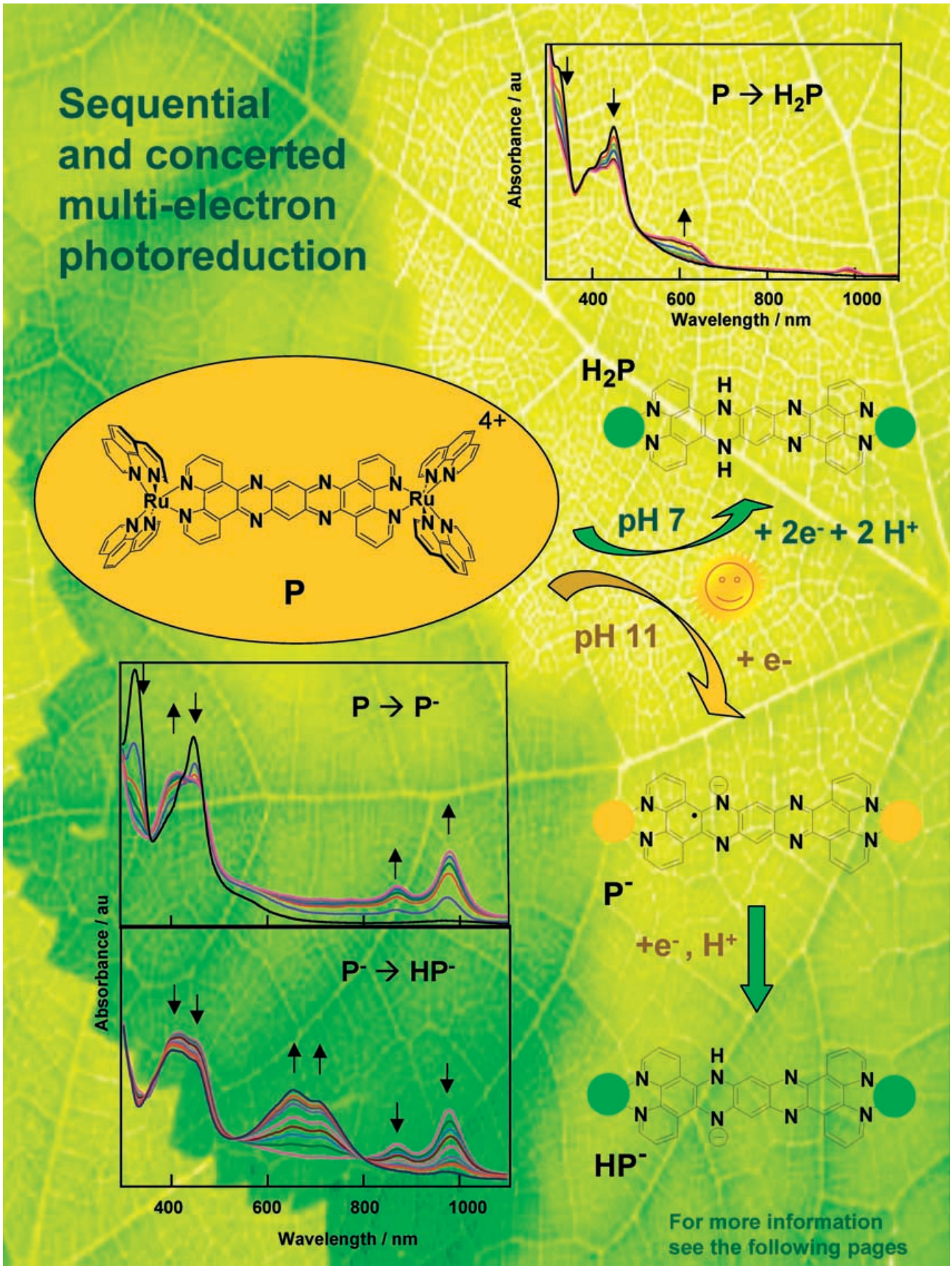

 DOI: 10.1002/chem.200401287

CHEMISTRY
A EUROPEAN JOURNAL

Influence of pH on the Photochemical and Electrochemical Reduction of the Dinuclear Ruthenium Complex, $[(phen)_2Ru(tatpp)Ru(phen)_2]Cl_4$, in Water: Proton-Coupled Sequential and Concerted Multi-Electron Reduction

Norma R. de Tacconi,[a] Reynaldo O. Lezna,[b] Rama Konduri,[a] Fiona Ongeri,[a] Krishnan Rajeshwar,[a] and Frederick M. MacDonnell*[a]

Abstract: The dinuclear ruthenium complex $[(phen)_2Ru(tatpp)Ru(phen)_2]^{4+}$ (**P**; in which phen is 1,10-phenanthroline and tatpp is 9,11,20,22-tetraaza tetrapyrido[3,2-a:2′3′-c:3″,2″-l:2‴,3‴]-pentacene) undergoes a photodriven two-electron reduction in aqueous solution, thus storing light energy as chemical potential within its structure. The mechanism of this reduction is strongly influenced by the pH, in that basic conditions favor a sequential process involving two one-electron reductions and neutral or slightly acidic conditions favor a proton-coupled, bi-electronic process. In this complex, the central tatpp ligand is the site of electron storage and protonation of the central aza nitrogen atoms in the reduced products is observed as a function of the solution pH. The reduction mechanism and characterization of the rich array of products were determined by using a combination of cyclic and AC voltammetry along with UV-visible reflectance spectroelectrochemistry experiments. Both the reduction and protonation state of **P** could be followed as a function of pH and potential. From these data, estimates of the various reduced species' pK_a values were obtained and the mechanism to form the doubly reduced, doubly protonated complex, $[(phen)_2Ru(H_2tatpp)Ru(phen)_2]^{4+}$ (**H_2P**) at low pH (≤ 7) could be shown to be a two-proton, two-electron process. Importantly, **H_2P** is also formed in the photochemical reaction with sacrificial reducing agents, albeit at reduced yields relative to those at higher pH.

Keywords: electron transfer · N ligands · photochemistry · reduction · ruthenium

Introduction

The ability to capture and store solar energy as easily usable chemical energy is an increasingly important research problem as the human demand for energy continues to grow and most existing sources are nonrenewable.[1] Ruthenium–polypyridyl complexes remain one of the most widely studied chromophores for molecular light-to-chemical energy conversion, because of their favorable photophysical properties and chemical stability.[2–4] Considerable progress has been made in the development of antenna-like structures that collect light energy and funnel it to a single site,[5–9] as well as molecular diad and triad architectures[9–15] that direct charge separation within the excited-state complex. Until recently, nearly all such assemblies were limited to storing a single photoexcited electron, the notable exception being a Ru-Ir-Ru trimer reported by Brewer and co-workers in 1994.[16] In 2002, we reported that the dinuclear Ru^{II} complex **P** and a closely related quinone analogue were capable of reversibly storing two to four electrons, respectively, upon visible-light irradiation in the presence of sacrificial reducing agents in acetonitrile.[17] The bridging ligands in these complexes have been shown to play the role of electron acceptor for the

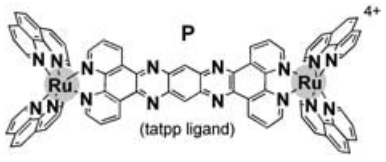

[a] Prof. N. R. de Tacconi, Dr. R. Konduri, F. Ongeri, Prof. K. Rajeshwar, Prof. F. M. MacDonnell
Department of Chemistry and Biochemistry
The University of Texas at Arlington
Arlington, TX 76019–0065 (USA)
Fax: (+1) 817-272-3808
E-mail: macdonn@uta.edu

[b] Prof. R. O. Lezna
INIFTA, CONICET-Universidad Nacional de La Plata
CC. 16, Suc. 4, La Plata (B1906ZAA) (Argentina)

DOI: 10.1002/chem.200401287

photoinduced charge-separation process and the role of the multi-electron storage unit. Their ability to also accept protons suggested that these "electron reservoirs" may ultimately be capable of driving proton-coupled, multi-electron-transfer reactions of the type desired for facile H_2 production or O_2 reduction, for example.

We identified all of the photochemically relevant redox and protonation states of the tatpp bridging ligand in **P** and showed that the photochemical activity was retained when water was added to solution in acetonitrile (1:4 H_2O/MeCN) as long as basic conditions were maintained.[18] Significantly, **P** was also shown to store up to four electrons on the bridging tatpp ligand by means of electrochemical reduction.

In this paper, we show that pure water can be used as the solvent for multi-electron photochemical processes and, by means of a combination of voltammetry and differential reflectance spectroelectrochemistry, we are able to probe the mechanism of reduction and protonation of **P** as a function of pH in the range 6 to 11. Clearly, water is the most desirable solvent to work with and is the ideal substrate for most light-to-chemical energy conversion schemes with dihydrogen and dioxygen as the photochemical products.

Results

Ladder scheme: A ladder scheme for the reduction and protonation of **P** is shown in Scheme 1. This scheme contains not only each individual chemical structure, but also its notation (**P**, $\mathbf{P}^-$, $\mathbf{P}^{2-}$, **HP**, $\mathbf{HP}^-$, and so on). The electron-transfer processes are presented vertically, while protonation/deprotonation processes are presented horizontally. While this notation is useful, it is worth noting that **P** is a large metal complex (over 2 nm long) carrying an overall +4 charge. Moreover, many of the isomers can exist in multiple tautomeric forms; however, the tautomers shown in this scheme are those chosen from a comparison with the tautomers established for various redox isomers of tetraazapentacene.[19]

UV-visible absorption spectra for P and reduction products: It is critical to have a clear understanding of the absorption spectra of the species presented in Scheme 1 if we are to successfully interpret the photochemical and spectroelectrochemical data. We have previously reported the absorption spectra for many of the nonprotonated and protonated species in MeCN[18] and can show that relatively minor shifts in peaks position and intensity occur as water is added to the mixture. Similarly, the absorption spectra of many of the redox and protonation states of 5,7,12,14-tetraazapentacene are known.[19,20] Figure 1 shows the spectra of $[Ru(phen)_3]^{2+}$, the Zn^{II} complex of tatpp, and **P** in MeCN. The absorption spectrum of **P** can be seen to simply be the sum of its components with two $[Ru(phen)_3]^{2+}$-type chromophores overlapping with the ligand centered transitions observed for "free" tatpp. In this case, the free "tatpp" spectrum is actually that of the Zn^{II} complex, as it is necessary to add a metal ion to solubilize the ligand. The Zn^{II} complex is free of any MLCT-type transitions and the observed LC transitions are likely only to be slightly perturbed by the Zn^{II} coordination. The molar extinction coefficients for these two components, $[Ru(phen)_3]^{2+}$ and tatpp, at 445 nm in MeCN are 19200[21] and 17300 $M^{-1}\,cm^{-1}$, respectively. A summation of the molar extinctions for these three components, two $[Ru(phen)_3]^{2+}$ and one tatpp, gives an ε_{445} of 55700 $M^{-1}\,cm^{-1}$ that compares reasonably well with the observed extinction coefficient for **P** of 65100 $M^{-1}\,cm^{-1}$ at 445 nm in MeCN,[22]

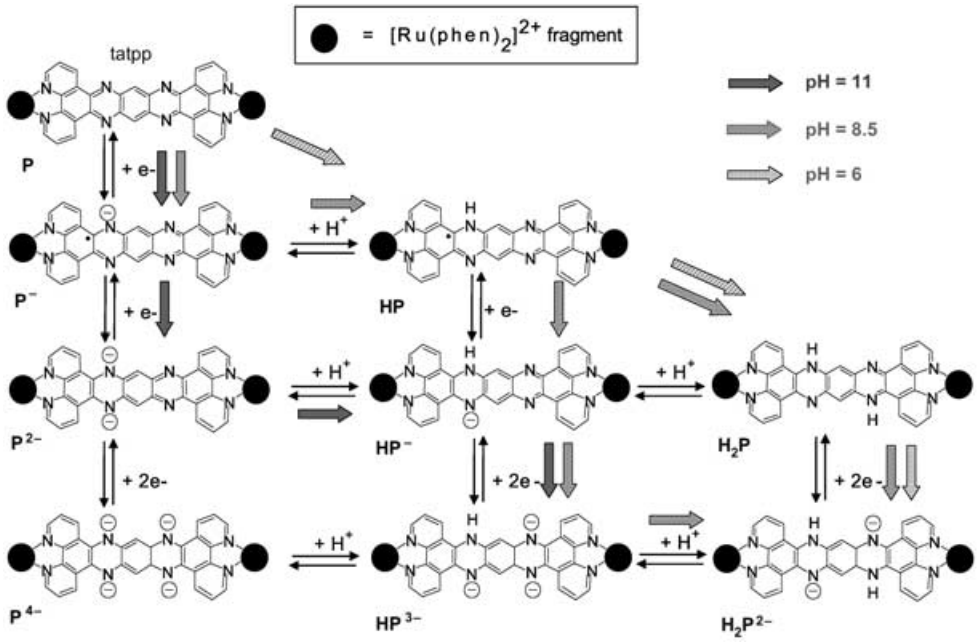

Scheme 1. Ladder diagram for the electronation and protonation processes for **P** in water at pH 11, 8.5, and 6.

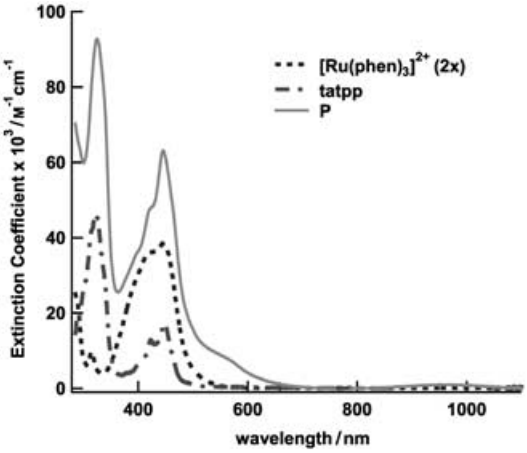

Figure 1. UV-visible electronic spectra (MeCN) of [**P**][PF_6]$_4$, [Ru(phen)$_3$]-[PF_6]$_2$, and tatpp ligand plus excess Zn(BF_4)$_2$ salt.

and the sharp bands with vibronic fine structure characteristic of the free ligand are clearly visible. The fact that all three chromophores are largely additive suggests relatively weak electronic coupling. Cyclic voltammetry (CV) data for **P** shows a single $Ru^{2+/3+}$ couple supporting the weak electronic coupling between metal centers, and the absorption spectra (vide infra) suggest better but still modest electronic coupling between metal chromophores and the tatpp LC chromophore. One additional, more intense LC band at 335 nm is observed in the Zn^{II}-tatpp complex as well as in **P** and is clearly only slightly perturbed by the coordination of the Ru^{II} fragments to the tatpp ligand.

As seen in Figure 2 (top), significant changes in the LC transitions at 335 and 445 nm are observed upon reduction to $\mathbf{P}^-$, $\mathbf{P}^{2-}$, and $\mathbf{P}^{4-}$ in MeCN. The first two were prepared by chemical reduction and the last one was generated electrochemically in situ (see below). All of the species, show characteristic Ru–phen-type (dπ–π*) MLCT's at ~440 nm, but each is uniquely defined by sharp LC transitions in the visible region. The singly ($\mathbf{P}^-$) and doubly ($\mathbf{P}^{2-}$) reduced forms are characterized by new LC absorptions at longer wavelengths (855 and 965 nm for $\mathbf{P}^-$ and 635 and 685 nm for $\mathbf{P}^{2-}$), which show vibronic fine structure like the 445 nm absorption for **P**. The quadruply reduced complex ($\mathbf{P}^{4-}$), however, is largely featureless with only a weak broad absorption at 440 nm, showing that even the intensity of the Ru–phen (dπ–π*) MLCT has been lessened.

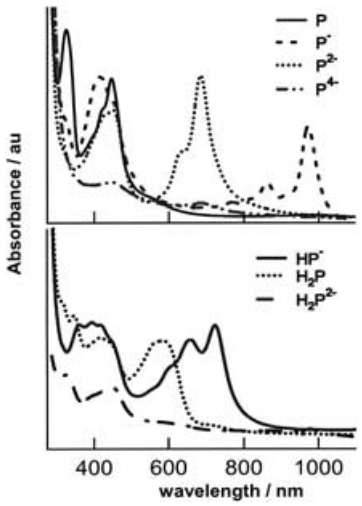

Figure 2. UV-visible electronic spectra (MeCN) of **P**, $\mathbf{P}^-$, $\mathbf{P}^{2-}$, and $\mathbf{P}^{4-}$ (top) and $\mathbf{HP}^-$, $\mathbf{H_2P}$ and $\mathbf{HP_2}^{2-}$ (bottom).

Absorption spectra for the protonated complexes $\mathbf{HP}^-$, $\mathbf{H_2P}$, and $\mathbf{H_2P}^{2-}$ are shown in Figure 2 (bottom). Stoichiometric protonation of $\mathbf{P}^{2-}$ gives $\mathbf{HP}^-$ and is characterized by the appearance of a third band in the spectrum of $\mathbf{P}^{2-}$ at 715 nm and a slight blue shift of the other LC bands to 655 and 608 nm. The relative heights of these three components were found to vary with the proton concentration, with the 715 nm band showing the strongest dependence on the [H^+]. Addition of another equivalent of H^+ yields $\mathbf{H_2P}$, in which the LC transitions now appear as a broad peak at 580 nm. $\mathbf{H_2P}$ can be further reduced by two electrons electrochemically, presumably leading to $\mathbf{H_2P}^{2-}$, and is characterized by the complete bleaching of the 580 nm LC band and partial bleaching of the 445 nm MLCT band. Appropriate wavelengths were selected from these spectra to follow the evolution of the absorption spectra as a function of potential in the differential reflectivity measurements in water. We note that the complex is readily soluble in water when prepared as a chloride salt, [(phen)$_2$Ru(tatpp)Ru(phen)$_2$]Cl_4.

Electrochemistry and spectroelectrochemistry of P in water: In an effort to determine the redox and protonation behavior of **P** in water, a combination of AC voltammetry and differential reflectance spectroelectrochemistry were used. The AC voltammetry data in MeCN and water (pH 11 and 6) is shown in Figure 3. The top voltammogram (Figure 3a) was

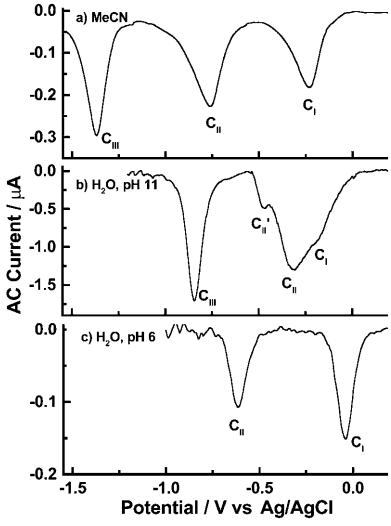

Figure 3. AC voltammograms for the electroreduction of **P** in acetonitrile (a), and in water at pH 11 (b) and 6 (c). The concentration of **P** was 2.5×10^{-5} M (a), 3.5×10^{-5} M (b), and 2.1×10^{-5} M (c).

obtained in dry MeCN and the waves correspond to two one-electron reductions (C_I, C_{II}) and one two-electron reduction (C_{III}) to generate $\mathbf{P}^-$, $\mathbf{P}^{2-}$, and $\mathbf{P}^{4-}$, respectively (vide infra). These data correspond well with the CV and differential pulse voltammetry (DPV) data obtained previously in MeCN.[18] In aqueous solution, the AC voltammograms show significant changes that are dependent on the pH, as contained in Figure 3b for pH 11 and Figure 3c for pH 6. The corresponding electroreduction processes are seen to occur at more positive potentials and in a narrower potential range, as may be expected for proton-coupled redox processes in a protic solvent. At pH 11 (Figure 3b), the first redox process shows three discernible features (C_I, C_{II}, and C'_{II}) that occur between 0.12 and −0.59 V, after which the doubly reduced product is obtained. The last redox process (labeled "C_{III}") is observed at −0.84 V and corresponds to a further two-electron reduction, as demonstrated by the spectroelectrochemical data.

At pH 6 (Figure 3c), only two redox processes (C_I and C_{II}) at −0.08 and −0.60 V versus Ag/AgCl, respectively, are detected and both processes involve a two-electron reduction as determined from a Randles–Sevcik analysis of the CV data for **P** (Figure 4). As seen in Figure 5, a plot of the

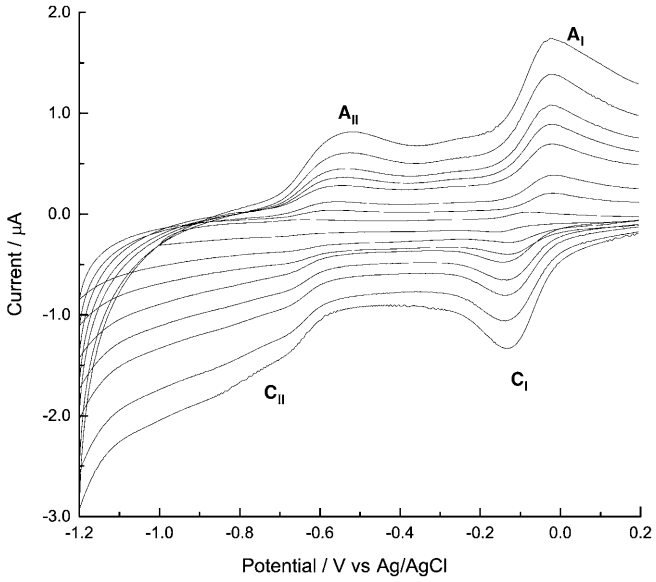

Figure 4. Cyclic voltammograms for the reduction of 8.0×10^{-5} M **P** in water at a 1.0 mm diameter gold disc electrode at scan rates of 10, 25, 50, 100, 150, 200, 300, and 400 mV s^{-1}. Supporting electrolyte: 0.2 M $Na_2B_4O_7$/0.15 M H_3BO_3 adjusted to pH 6 with 0.1 M H_2SO_4.

peak currents at C_I, A_I, and A_{II} for the CV data in Figure 4 versus the square root of the potential scan rate ($v^{1/2}$) shows good linearity for the defined waves (C_I, A_I, A_{II}) and is diagnostic of the diffusion-controlled nature of the electroreduction processes.[23] According to the Randles–Sevcik expression, the slope is proportional to the number of electrons exchanged in each process, assuming that both processes share the same diffusion coefficient (5.5×10^{-6} cm^{2}s^{-1}). All three

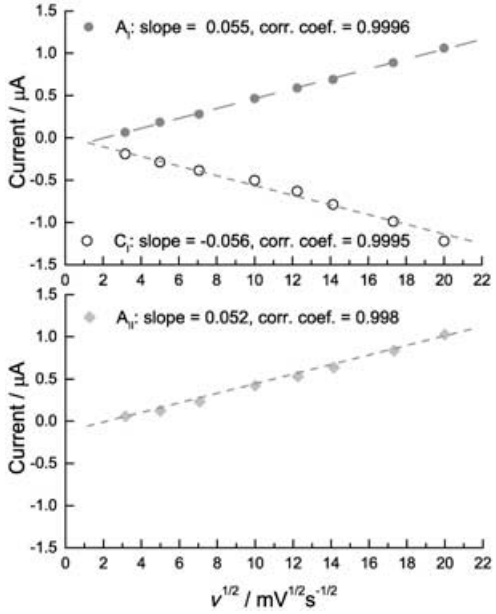

Figure 5. Randles–Sevick plots of peak current versus square root of potential scan rate for the data in Figure 4. The plot for C_{II} is not shown for reasons indicated in the text.

waves analyzed (C_I, A_I, and A_{II}) yield slopes corresponding to two-electron processes. As the cathodic portion of the second wave is poorly defined, it was not included in the analysis.

Figure 6 contains difference reflectance data between 350 and 800 nm at pH 11. The difference spectra obtained on changing the electrode potential from 0.2 V to −0.7 V

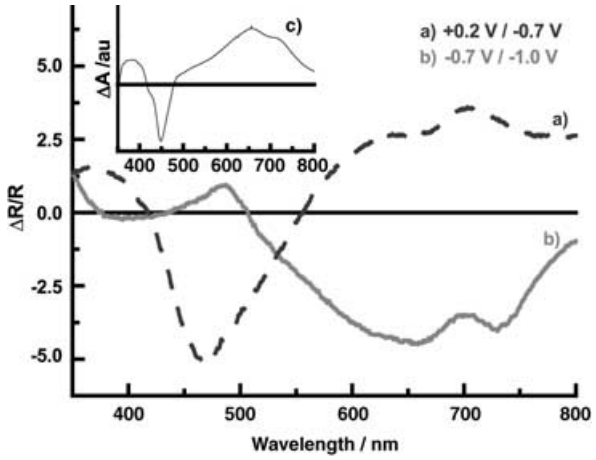

Figure 6. Modulated (difference) reflectance spectra for 2.5×10^{-5} M **P** at pH 11 on a mirror-polished gold electrode (area = 0.24 cm^2). Spectra were obtained by applying a square potential waveform at 11 Hz using two distinct potential regions: 0.2 V/−0.7 V (a), and −0.7 V/−1.0 V (b). The incidence angle of the light was 60°. Supporting electrolyte: 0.2 M $Na_2B_4O_7$/0.15 M H_3BO_3 adjusted at pH 11 with 0.1 M NaOH. The inset (c) contains a ΔA spectrum processed from data in Figure 11 showing the difference between the final photoproduct ($\mathbf{HP}^-$) and the initial **P** spectrum.

(curve a) and from −0.7 V/−1.0 V (curve b) are shown. Curve a encompasses the C_I, C_{II}, and C'_{II} redox process seen in Figure 3b and curve b encompasses the C_{III} redox process. The $\Delta R/R$ spectrum contains positive and negative contributions showing the intensity changes from the initial spectrum of **P**. The negative band at about 455 nm is the partial bleaching of the intense **P** absorbance, while the positive bands at approximately 650 and 710 nm are related to new species formed at potentials down to −0.7 V. The inset in Figure 6 (curve c) was obtained by subtracting the spectrum of **P** from the spectrum of $\mathbf{HP}^-$ in Figure 2. The similarity of the two profiles, a and c in Figure 6, suggests the same chemical species. Clearly the first set of overlapping reduction processes (C_I, C_{II}, and C'_{II}) yield the two-electron reduced product, predominantly as $\mathbf{HP}^-$, with a smaller fraction of $\mathbf{P}^{2-}$ also produced. In the second potential window (−0.7 to −1.0 V; curve b, Figure 6), the reflectance spectrum indicates bleaching of the bands at 655 and 715 nm and only a partial restoration of the 460 nm feature. This last reduction product shows the same spectral features, or more accurately, lack of spectral features as observed for $\mathbf{P}^{4-}$ generated in MeCN (Figure 2, top) and can reasonably be assigned as an additional two-electron reduction of $\mathbf{HP}^-$ in which the protonation state is not defined. This second, two-electron redox process is not observed photochemically, showing the photoreduction stops at the $2e^-$ stage (vide infra).

To probe the energetics of the conversion of **P** to its reduced products, differential reflectance spectroelectrochemistry (DRS) was used to follow the absorbance at selected wavelengths as a function of potential. Figure 7 contains data for **P** at pH 11 and at two wavelengths, 855 and 685 nm. These two wavelengths are unique for $\mathbf{P}^-$ (absorbing at 855 nm) and $\mathbf{HP}^-$ and $\mathbf{P}^{2-}$ (both absorbing at 685 nm, c.f., Figure 2). For the sake of clarity, the potential axis is now presented unfolded instead of pleated as is normally done in cyclic voltammetry. The scan starts at +0.15 V (rest potential) to −1.4 V and then back to +0.15 V. The polarity of the ordinate scale in Figure 7 is such that the appearance and disappearance of electrochemically generated products are represented by positive and negative $1/R\ \delta R/\delta E$ components, respectively, irregardless of the direction of the scan (positive- or negative-going).

As can be seen in Figure 7, the first species to appear is $\mathbf{P}^-$ (characterized by the absorption at 855 nm) and reaches a maximum rate of appearance at −0.25 V after which the rate slows considerably. Although the differential reflectance absorbance at 685 nm (curve "b") is observed to grow in slowly even while the 855 nm peak grows, its appearance is accelerated once the 855 nm absorbance begins to diminish and reaches a maximum absorbance at −0.48 V after which it begins to diminish. As the potential scan passes through the C_{III} redox process (Figure 3b), only a slight bleaching of the 685 nm absorbance is observed at approximately −0.8 V. Upon reaching the negative potential limit (−1.4 V) the scan is reversed and similar behavior is seen during the subsequent positive-going scan for both monochromatic curves, albeit with a higher absorbance (right frame of Figure 7) possibly indicating some adsorption/desorption process at the most negative potentials. The optical signals have the same sign during the negative- and positive-going scan, because the differential reflectance signal does not depend on the direction of the slow potential scan, but only on the δE perturbation.

At pH 8.5, the DRS data were acquired at 855 ($\mathbf{P}^-$), 715 ($\mathbf{HP}^-$), and 580 nm ($\mathbf{H_2P}$) as the speciation becomes more complex (see Figure 8). Additionally, the AC voltammogram is shown in Figure 8 (black dotted line) to indicate the correspondence between the optical and the electrical signals. Curve b, formation of $\mathbf{HP}^-$, is tracked now at 715 nm in order to be outside of any spectral tail from the band at 580 nm. The data show that $\mathbf{P}^-$ (curve a) is the first species to be formed, even though a clearly separated voltammetric wave is not observed. However, as the absorbance at

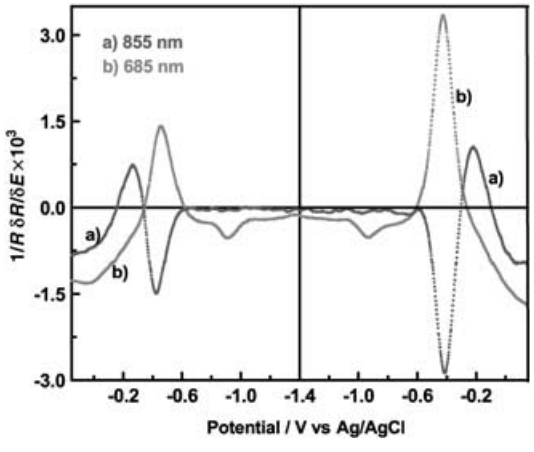

Figure 7. In-phase differential reflectance versus potential curves for 3.5×10^{-5} M **P** at pH 11 during a cyclic linear potential scan at 2 mV s^{-1} on a polycrystalline gold disk electrode. Two wavelengths were used to monitor the singly and doubly reduced products from **P**: a) 855 and b) 685 nm. The switch potential, −1.35 V, was used to separate the plot in two halves.

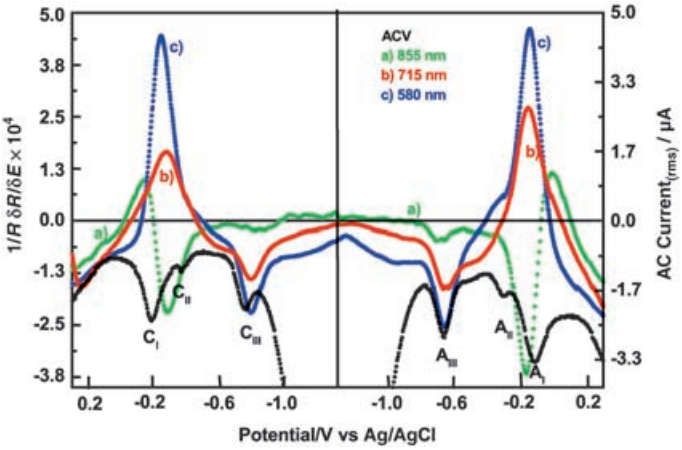

Figure 8. As in Figure 7 for 2.3×10^{-5} M **P** at pH 8.5, but three wavelengths were used: a) 855, b) 715, and c) 580 nm. Additionally, an AC voltammogram is shown superimposed to underline the correspondence between the optical and electrical signals.

855 nm reaches a maximum, we observe a strong increase in the 580 nm absorbance as well as in the 715 nm absorbance. $\mathbf{HP}^-$ actually starts appearing at potentials slightly more positive than $\mathbf{H_2P}$ and yet its maximum (rate of change of the $\delta R/\delta E$ at 715 nm) does not occur until slightly after the absorbance change at 580 nm ($\mathbf{H_2P}$) has maximized. It is also interesting to observe that the appearance of the doubly reduced product, $\mathbf{H_2P}$ as measured by the 580 nm trace, is essentially complete by the time the minor voltammetric peak C_{II} is reached. We suspect that this minor peak (C_{II}) is also associated with formation of $\mathbf{HP}^-$ (vide infra). At approximately −0.70 V, both the absorbances at 580 and 715 nm are bleached to some extent, corresponding well with the voltammetric wave C_{III} and the further reduction of the tatpp chromophore. No further changes are observed up to the negative potential limit (−1.4 V) and again the anodic scan is essentially a mirror image of the reduction except that slightly larger absorbance changes are observed. To eliminate the remote possibility that small contributions from the reflectance of the Au surface itself are interfering with the trends discussed above, the spectral measurements were repeated with a Pt working electrode, with identical results (the electroreflectance effect of Pt is known to be negligible).

Finally the differential reflectance spectra at 855 and 580 nm were obtained at pH 6.0 (Figure 9). At this pH only two species are observed, $\mathbf{P}^-$ and $\mathbf{H_2P}$, with the former only appearing in minor amounts relative to that observed at pH 8.5 and 11. Furthermore the appearance of both $\mathbf{P}^-$ and $\mathbf{H_2P}$ occurs nearly simultaneously, both of which are encompassed in a single voltammetric wave (C_I in Figure 3c). As the potential for the C_{II} process (Figure 3c) is reached the differential reflectance signal at 580 nm is almost completely bleached signaling further electroreduction of $\mathbf{H_2P}$ to the quadruply reduced species. The anodic scan (right frame of Figure 9) again shows the process is completely reversible.

The differential reflectance curves in Figure 8 were integrated and then normalized by the absorption coefficients of the corresponding species to yield the corresponding interfacial concentration, c_{int}, as a function of potential; Figure 10 contains the results. The first process at pH 8.5 is the formation of $\mathbf{P}^-$ (curve a); $\mathbf{P}^-$ then disappears to form $\mathbf{HP}^-$ (curve b) and $\mathbf{H_2P}$ (curve c). The disappearance of $\mathbf{P}^-$ in a restrained potential domain just after its appearance is responsible for the bipolar behavior for all the pHs studied. $\mathbf{H_2P}$ is formed in a broader potential domain than $\mathbf{P}^-$, but then recedes at potentials corresponding to the C_{III} wave (Figure 8). $\mathbf{HP}^-$ is also formed, albeit at lower amounts than $\mathbf{H_2P}$, and is seen to then decrease in the second potential region (−0.87/−1.4 V). The subsequent bleaching of the $\mathbf{H_2P}$ and $\mathbf{HP}^-$ bands is presumably related to the formation of the quadruply reduced $\mathbf{H_2P}^{2-}$ and/or $\mathbf{HP}^{3-}$ species. It is interesting to make a comparison with the electroreduction processes in acetonitrile (Figure 10, insert). Observe that the formation of $\mathbf{P}^-$ and its conversion to $\mathbf{P}^{2-}$ occurs in a more extended potential domain than in aqueous media, showing the reduction processes are facilitated in water, because of protonation. Furthermore, the bleaching of the peaks associated with the doubly reduced $\mathbf{P}^{2-}$ is also observed in MeCN when the C_{III} (Figure 3a) voltammetric process is reached, corresponding to formation of $\mathbf{P}^{4-}$ (see corresponding spectrum in Figure 2, top).

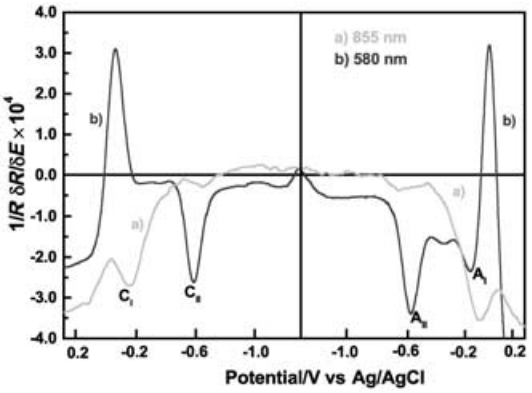

Figure 9. As in Figure 7 but for 2.1×10^{-5} M **P** at pH 6. Wavelengths are a) 855 and b) 580 nm. The voltammetric processes are labeled as C_I, C_{II} in the left frame and as A_{II} and A_I in the right frame, following the notation in Figure 3.

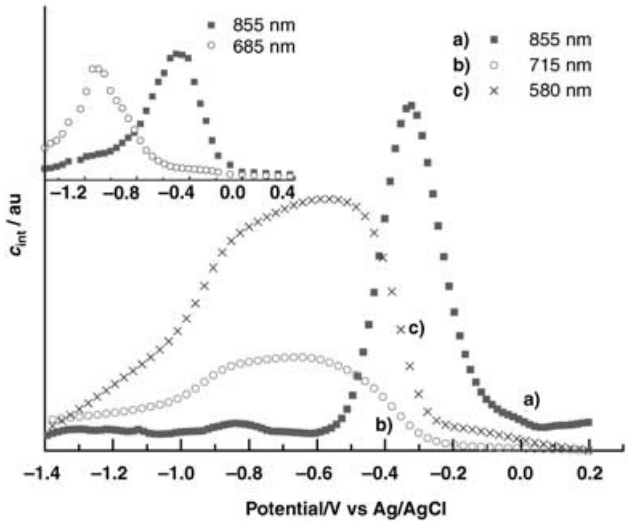

Figure 10. Interfacial concentration versus potential for $\mathbf{P}^-$, $\mathbf{H_2P}$, and $\mathbf{HP}^-$ at pH 8.5. The inset shows the fate of $\mathbf{P}^-$ and $\mathbf{P}^{2-}$ in acetonitrile in similar conditions.

Photochemistry of P in water: By using triethanolamine (TEOA) as a sacrificial reducing agent, we can examine the photochemistry of **P** in water at a variety of pH values including mildly acidic solutions, as the pK_b of 6.2 and TEOA[24] is high enough that an appreciable amount of the free amine is present even at pH 6. Complex **P** is photochemically active in water. Figure 11 shows the evolution of the absorption spectrum of **P** (16 μM) in an aqueous buffered solution containing TEOA (0.10 M) as it is irradiated

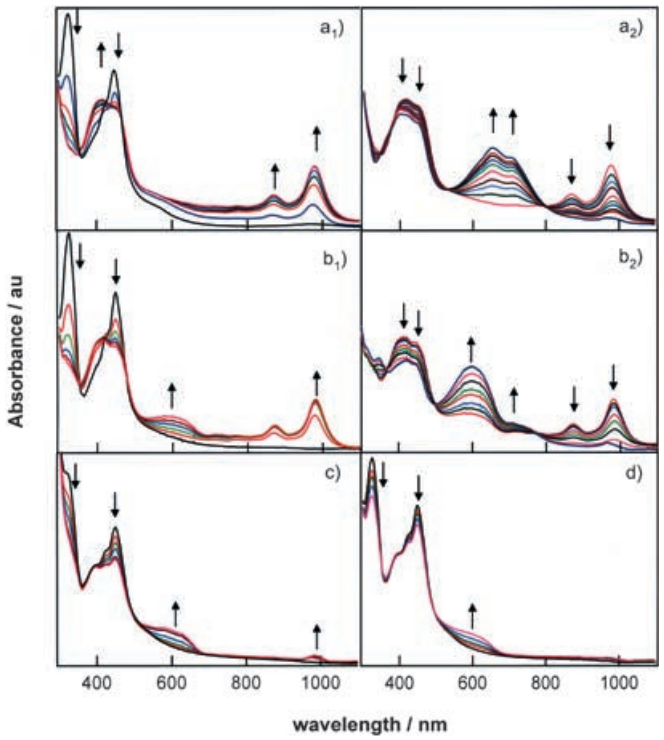

Figure 11. Evolution of the electronic spectrum of 15 μM **P** in water with added 0.25 M of TEOA during photolysisat four different pH values: pH 11 (a_1, a_2), pH 8.5 (b_1, b_2), pH 7.0 (c), and pH 6.0 (d).

with visible light ($\lambda > 330$ nm) at four different pH values: pH 11 (a_1, a_2), pH 8.5 (b_1,b_2), pH 7.0 (c), and pH 6.0 (d). At pH 11, we observe a small amount of $\mathbf{P}^-$ is formed prior to irradiation (see Figure 11a_1), with the black line indicating the solution spectra before addition of TEOA and the blue line immediately after. Irradiation, however, is required to complete the reduction and subsequently the long wavelengths peaks at 855 and 965 nm begin to diminish as peaks at 715 and 655 nm with a shoulder at 608 nm grow in (see Figure 11a_2). The second photoproduct can be assigned as a mixture of singly protonated, doubly reduced $\mathbf{HP}^-$ and the nonprotonated $\mathbf{P}^{2-}$ (c.f., Scheme 1).

At pH 8.5, no thermal reaction with TEOA is observed. Upon irradiation, the two long-wavelength peaks (855 and 965 nm) associated with $\mathbf{P}^-$ are observed to grow in with an additional broad feature appearing simultaneously at 580 nm. Eventually the long-wavelength peaks reach maxima and begin to diminish with a corresponding increase in the peak intensity at 580 nm, indicating conversion to $\mathbf{H_2P}$. The presence of a smaller shoulder at 715 nm shows that a small portion of $\mathbf{HP}^-$ is also formed in this photoreaction.

At pH 7.0, a very different picture is observed. Only a minor amount of $\mathbf{P}^-$ is ever formed and the broad absorption at 580 nm begins to appear immediately, indicative of $\mathbf{H_2P}$. Oddly, this peak never grows in to the same extent as that seen at pH 8.5. Moreover, the bleaching of the **P** absorptions at 370 and 444 nm is incomplete. This is even more apparent for the spectra obtained at pH 6.0. As seen in Figure 11d, no trace of $\mathbf{P}^-$ is ever observed and again the broad peak that appears at 580 nm never grows in to the same extent as at higher pH. There are several possibilities as to why $\mathbf{H_2P}$ does not fully form at lower pH including: 1) pH-induced aggregation which alters the photophysical behavior, 2) protonation events that deactivate the photoexcited state of the complex in a non-productive manner, and/or 3) the Ru chromophores and the TEOA reducing agent are unable to deliver two electrons simultaneously. Aggregation of these[25] and related types of complexes[20,26–30] is well established and has been observed to alter some physical properties. We have yet to systematically determine the effects of aggregation and electron stoichiometry but note that these effects may be addressable by synthetic modification of the structure (e.g., covalently tethering donor units to the Ru chromophores; overall charge modification). While further study is required here, it is clear that some $\mathbf{H_2P}$ can be produced under these conditions, demonstrating a bielectronic reduction and disprotonation of **P** without an observable monoreduced intermediate. We note that all of the photoproducts are cleanly reoxidized to the starting complex, **P**, upon exposure of the solutions to air.

Discussion

From both the current data and by comparison with the related Ru^{II} complexes of dipyridophenazine (dppz)[31–39] and tetrapyridophenazine (tpphz),[28,32,40,41] it is clear that complex **P** can be viewed as three weakly coupled molecular components; the two independent "Ru^{II}–trisbipyridine" chromophores and a central tetraazapenacene acceptor unit to form a chromophore-acceptor-chromophore triad. The additive nature of the absorption spectra for all three components, observed in Figure 1, reflects this nature. The ability of the tetraazapentacene ligand to accept multiple electrons stems from three properties:

1) The terminal acceptor orbital is poorly coupled to the Ru(dπ) orbitals, and this ultimate site of electron storage is not the acceptor orbital initially populated upon photoexcitation.
2) Multiple reduction states are accessible at potentials more positive than the terminal phen ligands (e.g., compare with Ru^{II} complexes of dppz[39] and tpphz[28]).
3) The central aza nitrogen atoms are easily accessible protonation sites.

By viewing the complex as an assembly of three molecular components we can interpret most of the observed spectral changes to reduction/protonation reactions of the tetraazapentacene unit.

Assignment of absorption spectra: Given the above description of the complex **P**, we can interpret the absorption spectra of the species shown in Scheme 1 by expanding on the

molecular orbital (MO) energy level diagram previously described, as shown Figure 12.[18] In this picture, all the absorptions in the visible portion of the spectra are either tetraazapentacene ligand-centered transitions ($\pi\rightarrow\pi^*$) or MLCT transitions of the type Ru(dπ)→"bipyridine"(π^*). Three tatpp-based orbitals, the HOMO−1 (π), LUMO (π_0^*), and LUMO+1 (π_1^*), and one metal-centered orbital, the HOMO (dπ), are required to develop a plausible MO diagram.

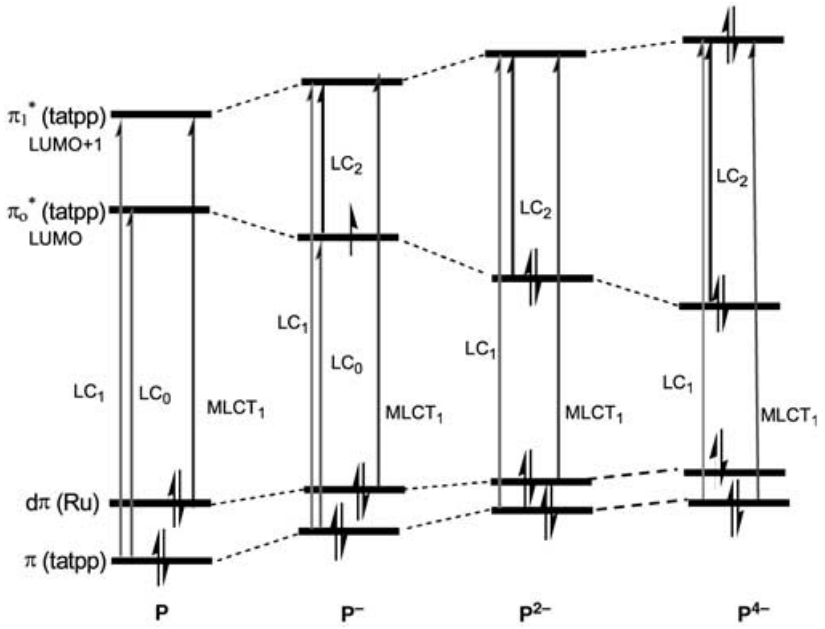

Figure 12. Partial molecular orbital energy diagram for **P**, $\mathbf{P}^-$, $\mathbf{P}^{2-}$, and $\mathbf{P}^{4-}$.

The π_1^* orbital of tatpp is much like the LUMO of a typical bipyridine or phenanthroline ligand (at both ends of the bridge) and is the orbital initially populated upon photoexcitation in the MLCT band, thus the broad absorption between 440 and 480 nm can be assigned, in part, to the Ru(dπ)→tatpp(π_1^*) transitions or $MLCT_1$.[18] The sharper transitions at 325 and 445 nm are also observed in the "free" tatpp spectrum (actually the Zn^{II}–tatpp complex in Figure 1) and are assigned as π–π_1^* (LC_1) and π–π_0^* (LC_0) transitions, respectively. Two similarly structured LC transitions are observed in the neutral and reduced forms of dppz[39] and tetraazapentacene.[20] We note that the π_0^* acceptor orbital is mainly centered on the tetraazapentacene portion of the triad and, as the overall LUMO, is the ultimate site of electron storage. The smaller, but not negligible, shoulder observed at 560 nm for **P** (see Figure 2, top) may represent the Ru(dπ)→(π_0^*) $MLCT_0$ transition. This transition is not typically observed in Ru^{II} complexes of the related dppz or tpphz ligands,[32] and is clearly not as favorable as the Ru(dπ)→(π_1^*) $MLCT_1$ transition for **P**. The exact nature of this absorption is still under investigation.

Upon reduction of **P** to $\mathbf{P}^-$, the π_0^* orbital is singly populated and a new low-energy LC transition becomes possible; this is labeled LC_2. The peaks at 855 and 965 nm represent this transition in which the splitting is due to vibronic fine structure. Further reduction to $\mathbf{P}^{2-}$ now fills the π_0^* orbital and results in additional nuclear rearrangements that stabilize the π_0^* orbital at the expense of the π_1^* orbital. This results in a blue shift for the LC_2 transition, which is now observed at 635 and 685 nm as a vibronically split pair. We observe that further reduction to $\mathbf{P}^{4-}$ in this model would fill the π_1^* orbital and bleach all the LC transitions; this is what is observed experimentally.

The effect of a single protonation of $\mathbf{P}^{2-}$ on this energy diagram would likely lead to further splitting of the energy levels associated with the pyrazine functions, consistent with the appearance of a new band at 715 nm appearing for $\mathbf{HP}^-$. The second protonation to form $\mathbf{H_2P}$ partially restores the ligand symmetry and the spectrum collapses and blue shifts to a single broad peak at 580 nm. More detailed calculations are required to fully explain all the spectral changes observed upon protonation, but it is clear that most of the species in Scheme 1 have unique bands in their absorption spectrum through which their presence can be followed spectroscopically.

The pK_a values for $\mathbf{P}^-$, $\mathbf{P}^{2-}$, and $\mathbf{HP}^-$: An estimate of the pK_a values of several important solution species indicated in reactions given in Equations (1)–(3) was obtained by analysis of the spectroelectrochemical data as discussed below.

$$\mathbf{HP} \rightleftharpoons H^+ + \mathbf{P}^- \quad pK_a \sim 8 \tag{1}$$

$$\mathbf{H_2P} \rightleftharpoons H^+ + \mathbf{HP}^- \quad pK_{a1} \sim 9 \tag{2}$$

$$\mathbf{HP}^- \rightleftharpoons H^+ + \mathbf{P}^{2-} \quad pK_{a2} \sim 10 \tag{3}$$

First, we observe that the parent complex **P** shows no appreciable change in its visible spectrum in water even at pH 0 and can infer that the tetraaza nitrogen atoms of tatpp are very weakly basic (or conversely the pK_a of $\mathbf{HP}^+ < 0$). At pH 11, the electroreduction of **P** to $\mathbf{P}^-$ is clean and only after complete formation of $\mathbf{P}^-$ are the subsequent products $\mathbf{P}^{2-}$ and $\mathbf{HP}^-$ produced. The fact that both $\mathbf{HP}^-$ and $\mathbf{P}^{2-}$ are present at this pH suggests we are close to the pK_{a2} value for the reaction in Equation (3) and as the predominant product is $\mathbf{P}^{2-}$ would suggest a lower value. We estimate a value of 10. At pH 8.5 (see Figure 8), it is clear that the predominant pathway for reduction is still through one-electron

steps, with $\mathbf{P}^-$ being the key intermediate. However, a small but detectable amount of $\mathbf{H_2P}$ is generated even at potentials positive of −0.25 V, at which formation of $\mathbf{P}^-$ dominates. In this range, we believe the $\mathbf{H_2P}$ formed is not a product of electrode reduction, but instead the result of protonation of $\mathbf{P}^-$ to form **HP**. This species, **HP**, is unstable with respect to disproportionation, as shown in the reaction given in Equation (4).[18]

$$2\,\mathbf{HP} \rightarrow \mathbf{H_2P} + \mathbf{P} \quad (4)$$

From these data, we can deduce that a small portion of $\mathbf{P}^-$ is protonated at this pH and then disproportionates, therefore the pK_a for the associated reaction 1 is close to, but less than, 8.5. Thus we estimate a pK_a of ~8 for **HP**. Interestingly, it had been shown that the doubly reduced form of $[Ru(bpy)_2(dppz)]^{2+}$ is generated in aqueous solution by means of a disproportionation reaction of the monoionic complex.[42]

Finally, we observe that both $\mathbf{HP}^-$ and $\mathbf{H_2P}$ are present in approximately a 30:70 ratio at pH 8.5 (Figure 8) showing we are close to, but below, the pK_{a1} for $\mathbf{H_2P}$, and therefore we estimate a pK_{a1} of ~9 for $\mathbf{H_2P}$. Finally, at pH 6 the only significant product is $\mathbf{H_2P}$, showing that we are well below the pK_a values for reactions (1)–(3).

Single and multi-electron proton-coupled electron transfer (ET): It is clear from the AC voltammetry and DRS data that the mechanism of first two reductions on the coordinated tatpp bridge in **P** is strongly affected by the solution pH with high pH (≥11) favoring sequential one-electron reductions to $\mathbf{P}^-$ [Eq. (5)] and then $\mathbf{P}^{2-}$ [Eq. (6)] or $\mathbf{HP}^-$ [Eq. (7)] and neutral or acidic conditions (pH≤7) favoring a proton-coupled bielectronic process [Eq. (8)].[43,44]

$$\mathbf{P} + e^- \rightleftharpoons \mathbf{P}^- \quad (5)$$

$$\mathbf{P}^- + e^- \rightleftharpoons \mathbf{P}^{2-} \quad (6)$$

$$\mathbf{P}^- + e^- + H^+ \rightleftharpoons \mathbf{HP}^- \quad (7)$$

$$\mathbf{P} + 2\,e^- + 2\,H^+ \rightleftharpoons \mathbf{H_2P} \quad (8)$$

For example, the potentials for reactions in Equations (5) and (6) in MeCN are observed at −0.20 and −0.75 V, respectively, whereas the potentials for these same two reactions are shifted to −0.15 and −0.50 V at pH 11. This reversibility in both MeCN and protic environments is not characteristic of the related dppz-type complexes.[39,45] The availability of protons leads to a new couple at the intermediate potential of −0.30 V, which is seen to dominate the AC voltammogram at pH 11 (Figure 3b) and can be assigned to the proton-coupled ET reaction in Equation (7).

It is evident that as the pH is lowered further, all the reduction potentials are all shifted to more positive values and the overall potential window narrows as the voltammetric peaks begin to merge. At pH 8.5, the merging of the first two cathodic processes is nearly complete as only one major cathodic wave (C_I) is observed on the AC voltammogram (Figure 8) though curiously, $\mathbf{P}^-$, $\mathbf{HP}^-$, and $\mathbf{H_2P}$ are all distinctly observed spectrally (DRS) in the same potential window (−0.1 to −0.3 V). Stepwise reduction still predominates here, because of the clear observation of the monoreduced product in the DRS. Less noticeable, but equally important, is the broad wave in the AC voltammogram for C_I, which indicates at least two closely associated waves instead of one. Furthermore, as seen in Figure 10, the plot of species concentration versus potential clearly shows that most of the doubly reduced products are derived from the sequential reduction of **P** to $\mathbf{P}^-$ and then reduction and protonation of $\mathbf{P}^-$ [Eq. (9)]. The appearance of some $\mathbf{H_2P}$ at potentials above −0.25 V (see Figure 10) is likely due to the formation of a small amount of **HP** at this pH and disproportionation [Eq. (4)].

$$\mathbf{P}^- + e^- + 2\,H^+ \rightleftharpoons \mathbf{H_2P} \quad (9)$$

We note that the formation of $\mathbf{HP}^-$ [Eq. (7)] slightly lags that of $\mathbf{H_2P}$, as may be expected for a sequential process in which a more negative potential would be required to generate $\mathbf{HP}^-$ than $\mathbf{H_2P}$. The minor cathodic wave C_{II} in Figure 8 is likely to be associated with this process [Eq. (7)] and, while not quantitative, corresponds well with $\mathbf{HP}^-$ being the minor doubly reduced product (~30% compared to 70% $\mathbf{H_2P}$). Additionally, some $\mathbf{HP}^-$ may be the product of $\mathbf{H_2P}$ losing a proton in solution. At pH 6, the first two reductions are no longer distinct, but instead, have merged to form a single two-proton, two-electron wave at −0.05 V (see Figure 3c), ultimately corresponding to the reaction given in Equation (8).

Quadruply reduced products ($\mathbf{P}^{4-}$ and protonated analogues): The formation of the quadruply reduced products from the doubly reduced products of **P** was observed in aprotic media as well as aqueous solution and, not surprisingly, the reduction becomes much easier to accomplish as protons are introduced and the proton concentration increased. We have not been able to unambiguously assign the protonation state of this product, except when formed in dry MeCN, and therefore will not attempt to assign it here. We use $\mathbf{H}_x\mathbf{P}^{x-4}$ as the generic representation of this family of compounds, with the understanding that the aqueous species are most certainly protonated to some degree. Unlike the earlier reductive processes, the formation of $\mathbf{H}_x\mathbf{P}^{x-4}$ is always observed as a bielectronic process regardless of the solution pH or even the presence of protons [Eq. (10)].

$$\mathbf{P}^{2-} + 2\,e^- + x\,H^+ \rightleftharpoons \mathbf{H}_x\mathbf{P}^{x-4}\ (x = 0-4) \quad (10)$$

Upon going from aprotic media to pH 6 aqueous solution, the redox potential for Equation (10) shifts from −1.35 to −0.60 V. The presence of two bielectronic redox couples on the tatpp ligand leads to a similar type of ligand-based mixed valency recently as that reported by Bachmann and Nocera for zinc–porphyrinogen complexes,[46] except here

we see protonation is integral to the bielectronic nature of the first couple.

As with the formation of $\mathbf{P}^{4-}$ in MeCN, we always observe bleaching of the tatpp LC transitions in the spectra obtained for the quadruply reduced species at any pH, as was anticipated from the MO description of **P** presented in Figure 12. The amount of bleaching can appear small in some of the differential reflectance spectra, but note that this is deceptive and, as shown in Figure 10, the same data viewed in a normalized fashion with respect to concentration shows the bleaching is extensive. In no case, were any of the quadruply reduced products observed under photochemical conditions.

Energetics of the photoreaction: It is interesting to compare the energetics in this system with some earlier $[Ru(bpy)_3]^{2+}$ systems that use methylviologen (MV^{2+}) as an oxidative quencher and electron relay and TEOA as the electron donor.[47–50] The irreversible oxidation of TEOA prevents the nonproductive back-reaction and thus the net photochemical reaction in a solution of TEOA, $[Ru(bpy)_3]^{2+}$ and MV^{2+} can be reduced to Equation (11).

$$TEOA + MV^{2+} \xrightarrow{[Ru(bpy)_3]^{2+},\, h\nu} TEOA^{+} + MV^{1+} \quad (11)$$

In our system, the tatpp bridge replaces the MV^{2+} and thus acts as an internal acceptor capable of storing two electrons (and protons) giving the net photoreaction 12 at pH 7 [Eq. (12)].

$$2\,TEOA + \mathbf{P} \xrightarrow{2h\nu} 2\,TEOA^{+} + \mathbf{H_2P} \quad (12)$$

While the ΔE is greater for the reaction in Equation (11) than that in Equation (12) (-1.58 vs -0.95 V, respectively), the fact that two equivalents of electrons are stored in $\mathbf{H_2P}$ means that $+183\ kJ\,mol^{-1}$ of light energy was harnessed to drive the endothermic reaction compared to $+152\ kJ\,mol^{-1}$ for MV^{+}. Of course these numbers do not reflect the biphotonic requirements of Equation (12) and by this criterion less light energy was harvested. However, the key difference here is not the efficiency of energy harvesting but the fact that in $\mathbf{H_2P}$ both electrons are stored in a single site (or molecular orbital) and are thus capable of participating in concerted multi-electron reactions with certain substrates. Furthermore, protons are intimately involved in the reaction mechanism and are carried along with the reducing equivalents allowing access to additional proton-coupled electron-transfer reactions possibly not accessible with reductants, such as MV^{1+}.

Conclusion

In summary, the electroreduction of **P** in aqueous media is much more complex than its counterpart previously studied in acetonitrile[18] and proton-coupled electron transfer clearly plays an important role in the reduction mechanism for aqueous solution. The speciation observed spectroelectrochemically matches that observed photochemically with similar product distributions at similar pH's and thus we were able to interrogate the reaction mechanism of the photochemical reduction. The bold purple, green and red arrows in Scheme 1 summarize the reaction paths observed for **P** at pH 11, 8.5 and 6, respectively. For pH 11 and 8.5 distinct sequential one-electron and proton-coupled, one-reduction processes are observed, but begin to merge at $pH \leq 7$, such that only a coupled two-electron, two-proton process is seen. At all pH's the doubly reduced product undergoes another bielectronic reduction electrochemically but not photochemically. Importantly, it is possible to photochemically produce the doubly reduced, doubly protonated $\mathbf{H_2P}$ at neutral or mildly acidic pH and thus store energy in a product capable of driving proton-coupled, multi-electron-transfer reactions. The clean reoxidation of $\mathbf{H_2P}$ to **P** by oxidants such as O_2, is evidence that this complex could be used in a photocatalytic manner to drive such reactions.

Experimental Section

Chemicals: The synthesis and purification of **P** as the chloride salt are described elsewhere.[22] Other chemicals were of the highest purity commercially available and were used as received.

Photochemical reduction: All solutions were sealed in a quartz cuvette with a rubber septum and degassed for 10 min with nitrogen or argon gas prior to irradiation. The cuvettes were immersed in a water bath ($18 \pm 2\,^{\circ}C$) and irradiated using a 100 W tungsten bulb with a 360 nm cutoff UV filter. The photon flux was 1.125×10^6 lux as measured by a Lutron LX101 meter. The progress of the photochemical reaction was monitored by recording the absorption spectra after periodic removal of the cuvette from the water bath. Triethanolamine (TEOA) was used as the sacrificial electron donor.

Electrochemistry and spectroelectrochemistry: The cells for voltammetry and spectroelectrochemistry experiments have been described elsewhere.[51] Gold and platinum discs polished to a mirror finish were used as working electrodes. A Pt coil used as counterelectrode was placed in a separate cell compartment with a fritted end. The reference electrode was Ag|AgCl, satd. KCl and was used with a Luggin capillary to minimize uncompensated Ohmic resistance in the cell. Dioxygen was exhaustively removed from the working electrode compartment by bubbling purified nitrogen for at least 40 min prior to each experiment.

Reflectance spectroelectrochemistry was performed in two modes: difference and differential. In the difference mode, the reflectance (R) data were acquired during square-wave modulation with the potential limits of the square-function chosen to encompass each redox wave being probed.[52] The data are presented in $\Delta R/R$ versus wavelength format. Differential reflectance–potential profiles are very useful for the detection of active electrochemical species as a function of potential.[53–55] Monochromatic light (again with the wavelength carefully chosen to be characteristic of the species being probed) was reflected off the working electrode surface and the change of the beam intensity in response to an AC potential modulation was monitored, after demodulation, as a function of the DC electrode potential. The magnitude of the signal depended on the capability of the particular species to follow the potential modulation that was superimposed on the slow DC potential scan. The optical signal generated by the AC modulation can be represented by Equation (13),[52] in which E is the electrode potential and A is the optical absorbance.

$$\frac{1}{R}\frac{\delta R}{\delta E} = -\frac{1}{R}\frac{\delta A}{\delta c_{int}}\left|\frac{\delta c_{int}}{\delta E} + \frac{1}{R}\frac{\delta R}{\delta q}\frac{\Delta q}{\delta E}\right|_{AuER} \quad (13)$$

The first term in Equation (13) accounts for the potential modulation of the interfacial species at the electrode. It consists of the modulation of the interfacial concentration (δc_{int}) of the various species instigated by the δE potential perturbation. This in turn provokes a corresponding change in A through Fresnel's law. In this first term, the gold working electrode is only participating as a reflecting mirror. The second term accounts for the gold electroreflectance, that is, changes in the optical properties of the gold due to changes of its free-electron concentration.[52,56]

AC voltammetry[57] can be considered as the electrical counterpart to the differential reflectance spectroelectrochemistry experiment described above. In this case, the Faradaic current in response to a small-amplitude potential perturbation was monitored as a function of the scanned (DC) potential. Both types of measurements were performed at 11 Hz with either 5 $mV_{p\text{-}p}$ or 50 $mV_{p\text{-}p}$ sine waves superimposed on a slow (1 $mV\,s^{-1}$) potential scan. For the spectroelectrochemical measurements, the radiation reflected from the electrode surface was focused on a photomultiplier operating at constant current mode by a feedback system and a power supply. The resulting optical AC response (in phase component) was demodulated with a lock-in amplifier and processed as in-phase signal.[53]

The electrolyte pH was maintained at 6, 8.5, and 11 with $Na_2B_4O_7/H_3BO_3$ borate buffer. All experiments pertain to the laboratory ambient temperature (25 ± 2 °C).

Instrumentation: Cyclic voltammetry and AC voltammetry experiments were performed by using a PC-controlled potentiostat (CH Instruments, Electrochemical Analyzer). Differential reflectivity/potential ($1/R\ \delta R/\delta E$) measurements used a S20 photomultiplier operated at constant current mode by a feedback controlled system on a Kepco operational power supply (Model OPS 2000B). A lock-in amplifier (PAR Model 5210) was used to demodulate the optical AC response.[54,55]

Acknowledgements

We thank the American Chemical Society-Petroleum Research Fund, Type AC (FMM, KR), the Robert A. Welch Foundation (FMM), the National Science Foundation CHE-0101399 (FMM) and CONICET (RA), PIP # 657/98 (ROL) for partial support of this research. We thank Mr. Kelly Wouters for experimental assistance.

[1] M. Gratzel, J.-E. Moser, in *Electron Transfer in Chemistry*, *Vol. 5* (Ed.: V. Balzani), **2001**, pp. 589.
[2] V. Balzani, P. Ceroni, M. Maestri, C. Saudan, V. Vicinelli, *Top. Curr. Chem.* **2003**, *228*, 159.
[3] V. Balzani, S. Campagna, G. Denti, A. Juris, S. Serroni, M. Venturi, *Acc. Chem. Res.* **1998**, *31*, 26.
[4] E. C. Constable, *Chem. Commun.* **1997**, *12*, 1073.
[5] S. Serroni, S. Campagna, F. Puntoriero, F. Loiseau, V. Ricevuto, R. Passalacqua, M. Galletta, *Comptes Rendus Chimie* **2003**, *6*, 883.
[6] F. Scandola, R. Argazzi, C. A. Bignozzi, C. Chiorboli, M. T. Indelli, M. A. Rampi, *Supramolecular Chemistry* (Eds.: V. Balzani, L. De Cola), Kluwer Academic (The Netherlands), **1992**, p. 235.
[7] A. F. Morales, G. Accorsi, N. Armaroli, F. Barigelletti, S. J. A. Pope, M. D. Ward, *Inorg. Chem.* **2002**, *41*, 6711.
[8] L. M. Dupray, M. Devenney, D. R. Striplin, T. J. Meyer, *J. Am. Chem. Soc.* **1997**, *119*, 10243.
[9] S. Campagna, S. Serroni, F. Puntoriero, F. Loiseau, L. De Cola, C. J. Kleverlaan, J. Becher, A. P. Sorensen, P. Hascoat, N. Thorup, *Chem. Eur. J.* **2002**, *8*, 4461.
[10] E. Baranoff, J.-P. Collin, L. Flamigni, J.-P. Sauvage, *Chem. Soc. Rev.* **2004**, *33*, 147.
[11] N. D. McClenaghan, R. Passalacqua, F. Loiseau, S. Campagna, B. Verheyde, A. Hameurlaine, W. Dehaen, *J. Am. Chem. Soc.* **2003**, *125*, 5356.
[12] O. Johansson, H. Wolpher, M. Borgstroem, L. Hammarstroem, J. Bergquist, L. Sun, B. Kermark, *Chem. Commun.* **2004**, 194.
[13] M. Hissler, A. Harriman, A. Khatyr, R. Ziessel, *Chem. Eur. J.* **1999**, *5*, 3366.
[14] J. A. Treadway, P. Chen, T. J. Rutherford, F. R. Keene, T. J. Meyer, *J. Phys. Chem. A.* **1997**, *101*, 6824.
[15] N. Armaroli, *Photochem. Photobiol. Sci.* **2003**, *2*, 73.
[16] S. M. Molnar, G. Nallas, J. S. Bridgewater, K. J. Brewer, *J. Am. Chem. Soc.* **1994**, *116*, 5206.
[17] R. Konduri, H. Ye, F. M. MacDonnell, S. Serroni, S. Campagna, K. Rajeshwar, *Angew. Chem.* **2002**, *114*, 3317; *Angew. Chem. Int. Ed.* **2002**, *41*, 3185.
[18] R. Konduri, N. R. de Tacconi, K. Rajeshwar, F. M. MacDonnell, *J. Am. Chem. Soc.* **2004**, *126*, 11621.
[19] L. Sawtschenko, K. Jobst, A. Neudeck, L. Dunsch, *Electrochim. Acta* **1996**, *41*, 123.
[20] S. A. Jenekhe, *Macromolecules* **1991**, *24*, 1.
[21] A. S. Torres, D. J. Maloney, D. Tate, F. M. MacDonnell, *Inorg. Chim. Acta* **1999**, *293*, 37.
[22] M.-J. Kim, R. Konduri, H. Ye, F. M. MacDonnell, F. Puntoriero, S. Serroni, S. Campagna, T. Holder, G. Kinsel, R. Rajeshwar, *Inorg. Chem.* **2002**, *41*, 2471.
[23] A. J. Bard, L. R. Faulkner, *Electrochemical Methods*, Wiley, New York, **1980**.
[24] G. Borghesani, F. Pulidori, *Electrochim. Acta* **1984**, *29*, 107.
[25] K. Wouters, F. M. MacDonnell, unpublished results.
[26] E. Ishow, A. Gourdon, J.-P. Launay, C. Chiorboli, F. Scandola, *Inorg. Chem.* **1999**, *38*, 1504.
[27] E. Ishow, A. Gourdon, J.-P. Launay, *Chem. Commun.* **1998**, 1909.
[28] J. Bolger, A. Gourdon, E. Ishow, J.-P. Launay, *Inorg. Chem.* **1996**, *35*, 2937.
[29] M.-J. Kim, F. M. MacDonnell, M. E. Gimon-Kinsel, T. DuBois, N. Asgharian, J. C. Griener, *Angew. Chem.* **2000**, *112*, 629; *Angew. Chem. Int. Ed.* **2000**, *39*, 615.
[30] S. Campagna, Giannetto, S. Serroni, G. Denti, S. Trusso, F. Mallamace, N. Micali, *J. Am. Chem. Soc.* **1995**, *117*, 1754.
[31] E. Amouyal, A. Homsi, J.-C. Chambron, J.-P. Sauvage, *J. Chem. Soc. Dalton Trans.* **1990**, 1841.
[32] G. Pourtois, D. Beljonne, C. Moucheron, S. Schumm, A. Kirsch-De Mesmaeker, R. Lazzaroni, J.-L. Bredas, *J. Am. Chem. Soc.* **2004**, *126*, 683.
[33] B. Oenfelt, J. Olofsson, P. Lincoln, B. Norden, *J. Phys. Chem. A* **2003**, *107*, 1000.
[34] M. K. Brennaman, J. H. Alstrum-Acevedo, C. N. Fleming, P. Jang, T. J. Meyer, J. M. Papanikolas, *J. Am. Chem. Soc.* **2002**, *124*, 15094.
[35] B. Onfelt, P. Lincoln, B. Norden, J. S. Baskin, A. H. Zewail, *Proc. Natl. Acad. Sci. USA* **2000**, *97*, 5708.
[36] A. E. Friedman, J.-C. Chambron, J.-P. Sauvage, N. J. Turro, J. K. Barton, *J. Am. Chem. Soc.* **1990**, *112*, 4960.
[37] P. Lincoln, A. Broo, B. Norden, *J. Am. Chem. Soc.* **1996**, *118*, 2644.
[38] J. Olofsson, B. Oenfelt, P. Lincoln, *J. Phys. Chem. A.* **2004**, *108*, 4391.
[39] J. Fees, W. Kaim, M. Moscherosch, W. Matheis, J. Klima, M. Krejcik, S. Zalis, *Inorg. Chem.* **1993**, *32*, 166.
[40] C. Chiorboli, M. A. J. Rodgers, F. Scandola, *J. Am. Chem. Soc.* **2003**, *125*, 483.
[41] S. Campagna, S. Serroni, S. Bodige, F. M. MacDonnell, *Inorg. Chem.* **1999**, *38*, 692.
[42] Q. G. Mulazzani, M. D'Angelantonio, M. Venturi, M. L. Boillot, J. C. Chambron, E. Amouyal, *New J. Chem.* **1989**, *13*, 441.
[43] M. Mastragostino, L. Nadjo, J. M. Saveant, *Electrochim. Acta* **1968**, *13*, 721.
[44] R. I. Cukier, D. G. Nocera, *Annu. Rev. Phys. Chem.* **1998**, *49*, 337.
[45] M. Staffilani, P. Belser, L. De Cola, F. Hartl, *Eur. J. Inorg. Chem.* **2002**, 335.
[46] J. Bachmann, D. G. Nocera, *J. Am. Chem. Soc.* **2004**, *126*, 2829
[47] J.-M. Lehn, J.-P. Sauvage, R. Ziessel, *Nouv. J. Chim.* **1981**, *5*, 291.
[48] D. P. Rillema, G. Allen, T. J. Meyer, D. Conrad, *Inorg. Chem.* **1983**, *22*, 1617.
[49] M. Georgopoulos, M. Z. Hoffman, *J. Phys. Chem.* **1991**, *95*, 7717.

[50] I. Willner, R. Maidan, D. Mandler, H. Duerr, G. Doerr, K. Zengerle, *J. Am. Chem. Soc.* **1987**, *109*, 6080.
[51] R. O. Lezna, N. R. de Tacconi, J. A. Rapallini, A. J. Arvia, *An. Asoc. Quim. Argent.* **1998**, *76*, 25.
[52] R. O. Lezna, N. R. de Tacconi, A. J. Arvia, *J. Electroanal. Chem. Interfacial Electrochem.* **1988**, *255*, 251.
[53] E. Wolcan, M. R. Feliz, G. T. Ruiz, M. P. Juliarena, R. O. Lezna, *J. Electroanal. Chem.* **2002**, *533*, 101.
[54] R. O. Lezna, N. R. de Tacconi, A. J. Arvia, *J. Electroanal. Chem. Interfacial Electrochem.* **1990**, *283*, 319.
[55] R. O. Lezna, N. R. de Tacconi, S. Centeno, A. J. Arvia, *Langmuir* **1991**, *7*, 1241.
[56] W. N. Hansen, A. Prostak, *Phys. Rev.* **1968**, 500.
[57] C. M. A. Brett, A. M. O. Brett, *Electrochemistry: Principles, Methods, and Applications*, Oxford University Press, Oxford, **1993**.

Received: December 15, 2004
Published online: May 11, 2005

